Supplementary material for Hsu et al.,

Lhx2 regulates the timing of β-catenin-dependent cortical neurogenesis

Lea Chia-Ling Hsu[a,b,c,1], Sean Nam[a,1], Yi Cui[d], Ching-Pu Chang[a], Chia-Fang Wang[a], Hung-Chih Kuo[a], Jonathan D. Touboul[d,e], and Shen-Ju Chou[a,b,c,2]

[a]Institute of Cellular and Organismic Biology, Academia Sinica, Taipei, 115, Taiwan;
[b]Molecular Cell Biology, Taiwan International Graduate Program, Academia Sinica, Taipei, 115, Taiwan;
[c]Graduate Institute of Life Sciences, National Defense Medical Center, Taipei, 114, Taiwan;
[d]Collège de France, Centre for Interdisciplinary Research in Biology, CNRS UMR 7241, INSERM U1050, MemoLife Paris Science Lettres, Paris, 75231, France;
[e]Inria Paris-Rocquencourt, Mycenae Team, Le Chesnay 78153, France

[1]These authors contributed equally.

[2]Corresponding author

Shen-Ju Chou, schou@gate.sinica.edu.tw

Institute of Cellular and Organismic Biology, Academia Sinica

128 Academia Rd. Sec. 2, Taipei, Taiwan 115.

Including: Mathematical model and simulations, Materials and methods, Supplemental references and Figure S1-S10.

Mathematical Model and Simulations

In this section we provide the details of the mathematical model used to simulate the cortical development, and the algorithm used to perform the stochastic simulations.

System specification

The model only depends on the rate at which cortical progenitor cells divide (number of divisions per unit time) and how this rate depends on time and on the type of division. According to the previous studies, there are 4 main phases for cortical neurogenesis (S1):

(i) *Symmetric division* of the progenitor cells that occur at early stages of cortical development, with a rate $p_1(t)$ (see Figure S9A)

$$P \xrightarrow{p_1(t)} 2P$$

This is the unique phase associated with an increase of the number of progenitor cells. It constitutes the substrate upon which neurons and glia is formed, and therefore tightly regulates the size of the brain.

(ii) Asymmetric division of a progenitor cell into IPC (intermediate progenitor cell, or basal progenitors) with a rate $p\_2(t)$. IPCs subsequently divide and differentiate into two neurons

$$P \xrightarrow{p_2(t)} P + IPC \rightarrow P + 2N$$

Neurons formed at time t migrate to layer $l \in \{6,5,4,2/3\}$ with a time-dependent probability $q_l(t)$.

(iii) Asymmetric division of a progenitor cell into a progenitor and a neuron with a rate $p_3(t)$

$$P \xrightarrow{p_3(t)} P + N$$

Similar to phase (ii), the differentiation at time t gives rise to a neuron of layer l with probability $q_l(t)$.

(iv) The last phase taking place in the process of cortical development is the loss of capacity to generate a progenitor or a neuron. This phase, occurring at a rate $p_4(t)$, either corresponds to the formation of glial cells or to apoptosis.

$$P \xrightarrow{p_4(t)} \emptyset$$

Parameters fit

As mentioned in the main text, the only parameters to fit are the initiation and end times of the different phases $(p_\varphi(t), \varphi = 1 \cdots 4)$ as well as the probability for a neuron generated at time t to belong to layer l $(q_l(t), l \in \{6,5,4,2/3\})$. We consider that the probabilities p_φ and q_l have a typical profile $\varphi(t_{start}, t_{end}, t)$ only parameterized by their initiation (t_{start}) and end (t_{end}) times, and thus the model is complete once adjusted the start and end time of each phase. The map $t \mapsto \varphi(t_{start}, t_{end}, t)$ is a smooth step function. Results do not tightly depend on the choice of the function, and we fixed in our simulations:

$$\varphi(t_{start}, t_{end}, t) = (1 + \mathrm{erf}(t - t_{start})) \cdot (1 - \mathrm{erf}(t - t_{end}))$$

We chose the start and end times of each phase so that the end state fits the cell counts obtained for the WT cortex (Figure S1). We then varied these parameters in mutant scenarios to uncover what type of disruption may be consistent with the *Lhx2* cKO phenotype.

Mutant Models

The *Lhx2* cKO mice shows a significantly smaller cortex with approximate halving of the number of neurons in superficial layers and a reduction of 40% in deeper layers (Figure S1). The reduction of the cortical size is the result of a shorter duration of progenitor symmetric division phase. We adjusted to the duration of progenitor symmetric division phase to reach the reduction of cortical size in *Lhx2* cKO (Figure 5). We fitted the parameters in order to recover the correct cell counts in a given column. We started with an initial pool of $P_0 = 50$ progenitor cells (note that this acts only as a scale parameter and does not change qualitatively the outcome of the system). The parameters of the WT model (and other mutant scenarios) are provided in Table S1.

In order to illustrate how the different timings affect the cortical thickness and composition of the different layers, we further provide the four conceivable

scenarios with different disruption during neurogenesis (see Figure S9A and Table S1):

(i) Model M1: The switch from neurogenesis to gliogenesis is delayed (i.e. end of the neurogenesis and beginning of gliogenesis shifted by the same amount)

(ii) Model M2: Similar as M1 except that the switch is advanced

(iii) Model M3-M4: gliogenesis onset only is advanced (more dramatically in M4)

	End of symmetric division	Neurogenesis start	Neurogenesis end	Gliogenesis
WT	**5**	**5**	**10**	**10**
MUT	**3**	**3**	**8**	**6**
M1	5	5	12	12
M2	5	5	8	8
M3	5	5	10	8.5
M4	5	5	10	6

Table S1 Parameters used in Figure S9, The WT and MUT models are used in the main text (Figure 5).

The cortical thickness is evaluated as the number of neurons generated by a progenitor and it is thus proportional to the number of neurons produced: It increases when the duration of neurogenesis phase is longer (model M1) or decreases when the duration of neurogenesis is shorter (model M2). The cortical thickness t is also sensitive to the onset of gliogenesis: the earlier the gliogenesis, the thinner the resulting cortex (Fig. S9B). If both neurogenesis termination and onset of gliogenesis are shifted, the proportions of neurons in the different layers are unchanged (models M1 and M2, Fig. S9C), but as soon as gliogenesis is advanced during neurogenesis phase, the proportions of neurons in the superficial layers is reduced. The level of this phenomenon depends on how advanced gliogenesis is (only L2/3 for M3, both L4 and L2/3 for M4).

Simulation Algorithm

The simulations were performed using so-called the Doob-Gillespie algorithm (S2) for exact simulation of cell divisions. Given the rate of division of progenitor cells, it draws the time of the division, which is an exponential random variable with parameter given by the total rate of division $\Pi(t) = \sum_{i=1}^{4} p_i(t)$ multiplied by the number of progenitors cells at time t, $P(t)$. Once the time of the next event is found, the division occurring is chosen with a probability equal to the ratio between the rate of this event and the total rate: $P(t)/\Pi(t)$, and if a neuron is created, it is attributed to layer l with probability $q_l(t)$. The simulations start with an initial pool of progenitors P_0 and are run until all progenitors have lost their capacity to generate neurons (or when neurogenesis is stopped). All simulations were performed in Matlab®, using a code that we developed for the purpose of this article.

Materials and methods

Animals

Timed pregnant mice were used in accordance with Academia Sinica institutional guidelines. The day of insemination and day of birth are designated as embryonic day 0.5 (E0.5) and postnatal day 0 (P0), respectively. Genotyping for the *Lhx2* floxed*, Nestin*-cre and the BAT-gal alleles was performed using the polymerase chain reaction (PCR), as previously described (20, 21).

Cell culture and Luciferase reporter assay

The 293T cell line was cultured in medium that contained DMEM (Life Technologies) supplemented with 10% fetal bovine serum. For luciferase assays, cells were plated in 12-well plates and transfected the next day with luciferase reporters and a *Renilla* luciferase vector to normalize transfection efficiency. The transfection was performed using Lipofectamine transfection reagent according to the manufacturer protocol (Life Technologies). The cells were harvested 48 h after transfection and processed using the Dual-Glo Luciferase Assay System (Promega). The data were obtained in from three independent experiments.

Histochemistry

For immunostaining and X-Gal staining, brains were fixed in 4% PFA in PBS, cryoprotected in 30% sucrose/PBS, cut in 20 µm sections, and stained as described (20, 21). Antibodies used were: rat anti-BrdU (Accurate), goat anti-Brn2 (Santa Cruz), rabbit anti-Ctip2 (Novus), EdU (Click-iT EdU Imaging kit, Life Technologies), mouse anti-GFAP (cell signaling), rabbit anti-GFP (Life Technologies), mouse anti-Reelin (Millipore), mouse anti-Satb2 (Abcam), rabbit anti-Sox2 (Millipore), rabbit anti-Tbr1 (Abcam) and mouse anti-TuJ1 (Covance). Cell counts were made on coronal section images at matching rostral-caudal and medial-lateral levels. Statistical comparisons of cell counts in mutant and control mice were made using a paired *t*-test. TUNEL (terminal deoxynucleotidyl transferase–mediated deoxyuridinetriphosphate nick end-labeling) assay was performed with In Situ Cell Death Detection Kit (Roche).

***In situ* hybridization**

Brains were fixed with 4% paraformaldehyde in PBS, cryoprotected with 30% sucrose in 0.1 M PBS, embedded in Tissue Tek OCT compound (Sakura Finetek) and cut in 20 µm sections on a cryostat. *In situ* hybridization using digoxigenin (DIG)-labeled riboprobes was undertaken as described (20, 21).

***In utero* electroporation**

Expression construct CAG-GFP was made by subcloning GFP into a pCAG vector containing the cytomegalovirus (CMV) early enhancer element and chicken β-actin promoter. Nes-act-βCat was generated by subcloning the constitutively active β-catenin (chicken β–Cat with first 47 amino acid truncation) into the Nestin enhancer and hsp68 promoter containing vector. *In utero* electroporation was performed as described (S3). In short, E13.5 embryos were visualized through the uterus using a fiber optic light source. DNA solutions containing 0.25 µg/µl pCAG-GFP +/- 0.75 µg/µl Nestin-ActβCat + 1% fast green (Sigma) were injected with a glass capillary into the ventricle of each embryo and electroporated with Paddle-type electrodes (CUY21 Electroporator: Nepa Gene) in a series of five square-wave current pulses (35 V, 100 ms × 5). Electroporated embryos were allowed to develop until E15.5 and selected for further analyses by direct visualization of GFP expression.

The distribution of eGFP-expressing cells was assessed by immunostaining with anti-GFP antibody.

Pair-Cell Analysis

Clonal culture and pair-cell analysis were done as described previously (S4). Briefly, the cortices of WT or *Lhx2* cKO embryos at E12.5 were dissected and dissociated in single clones. Single cells were plated in poly-L-lysine coated 60-well Terasaki plates incubated. Pair cells were identified after 24 hours of incubation and were fixed with 4% PFA and stained with DAPI, TuJ1 and Sox2 antibodies.

Quantitative RT-PCR

Total RNA from the dTel of E12.5 WT and cKO brains was extracted using Trizol (Life Technologies). Reverse transcription was performed using Superscript III (Life Technologies). 1 µg of total RNA was reverse transcribed using random hexamers. Quantitative PCR (qPCR) was performed using the SYBR Green PCR Master Mix (Life Technologies). 18sRNA transcripts served as a normalizing control. All samples were tested in triplicate. For all qPCR analyses, RNA from three independent replicates for both WT and cKO dTel were examined. Error bars represent STDEV. Primers used for qPCR analyses were:

Lhx2	AAGCTCAACCTGGAGTCGGAA	TGAGGTGATAAACCAAGTCCCG
Tis21	GCGAGCAGAGACTCAAGGTT	CCAGTGGTGTTTGTAATGATCG
Hes6	ATGAGGTGCACACGTTCG	GCAGCGGCATGGATTCTA
Blbp	TAAGTCTGTGGTTCGGTTGG	CCCAAAGGTAAGAGTCACGAC
Tnc	GGGCTTTGACTGTAGTGAGAT	CATCACAGATACACATGCCATTC
Pax6	GCCCTTCCATCTTTGCTTGGGAAA	TAGCCAGGTTGCGAAGAACTCTGT
18sRNA	GAGGCCCTGTAATTGGAATGAG	GCAGCAACTTTAATATACGCTATTGG

Supplementary References

(S1) Kwan, K.Y., Sestan, N, Anton, E.S., (2012). Transcriptional co-regulation of neuronal migration and laminar identity in the neocortex. Development 139, 1535-1546.

(S2) Gillespie, D.T., (1977). Exact Stochastic Simulation of Coupled Chemical Reactions. The Journal of Physical Chemistry 81 (25): 2340–2361.

(S3) Li, H., Chou, S.J., Hamasaki, T., Perez-Garcia, C.G., O'Leary, D.D., (2012). Neuregulin repellent signaling via ErbB4 restricts GABAergic interneurons to migratory paths from ganglionic eminence to cortical destinations. Neural development 7, 10.

(S4) Sahara S & O'Leary DD (2009) Fgf10 regulates transition period of cortical stem cell differentiation to radial glia controlling generation of neurons and basal progenitors. *Neuron* 63(1):48-62.

Supplementary Figures

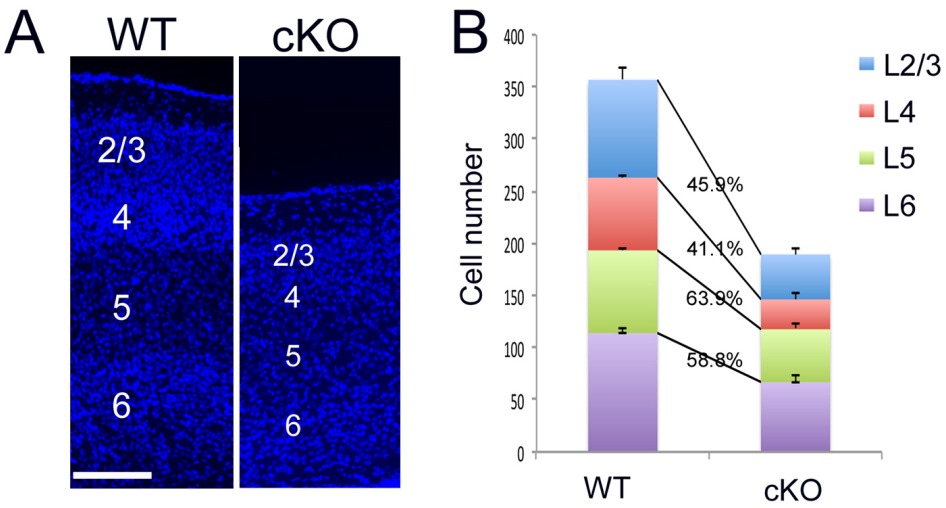

Figure S1 Comparison of the thickness of cortex and of each cortical layer in WT and cKO mice. (A) DAPI staining of coronal sections of P7 WT and cKO cortices. (B) Histogram showing the numbers of neurons in P7 WT and cKO cortices in a 100μm wide column. Relative to WT (layers (L)2/3, 93.7+/-12.9; L4, 69.7+/-4.9; L5, 79.3+/-1.5 and L6, 114.0+/-5.0; n=3), the number of cortical neurons in each layer in the cKO mouse is significantly decreased (P<0.05 by an unpaired Student's t-test) (L2/3, 43.0+/-6.0; L4, 28.7+/-4.0; L5, 50.7+/-5.8 and L6, 67.0+/-6.1; n=3). The number of neurons in cKO (189.3, n=3) is 53.1% of that in the WT (356.7, n=3). The neuronal number in each cortical layer is differentially affected; the deep layers (L5 and L6) are less affected than the superficial layers (L2/3 and L4). Scale bar, 100μm.

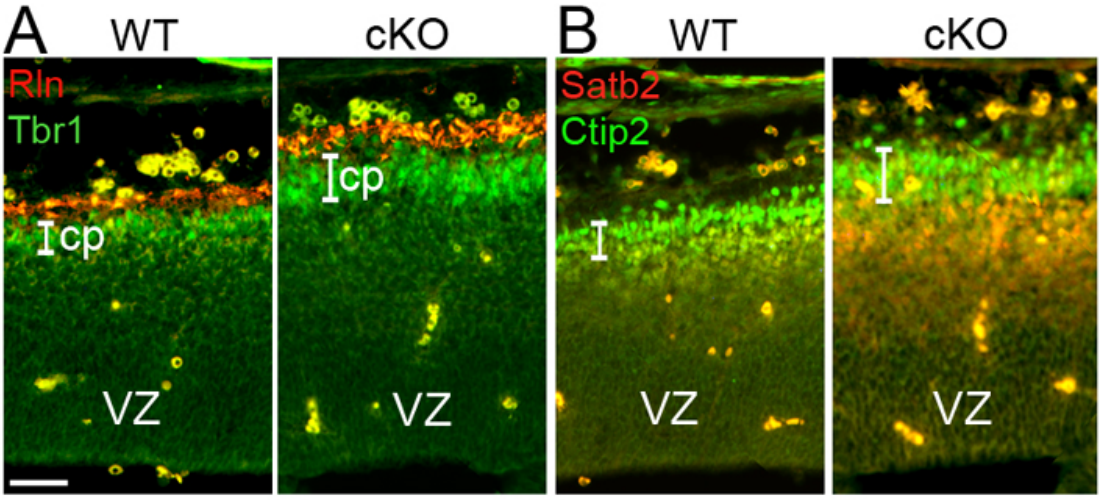

Figure S2 Precocious neurogenesis in *Lhx2* cKO mice. (A) Immunostaining for Reelin (Rln) and Tbr1 on coronal sections of E13.5 WT and cKO dTel. Reelin (red) labels Cajal-Retzius neurons in the marginal zone, and Tbr1 labels the cortical plate (cp). (B) Immunostaining for Ctip2 and Satb2 on coronal sections of E13.5 WT and cKO dorsal telencephalon. Ctip2 (green) labels newly born layer 5 neurons in the cortical plate. A greater number of Satb2-labeled superficial neurons are seen in the cKO relative to WT dTel. VZ, ventricular zone. Scale bar, 100μm.

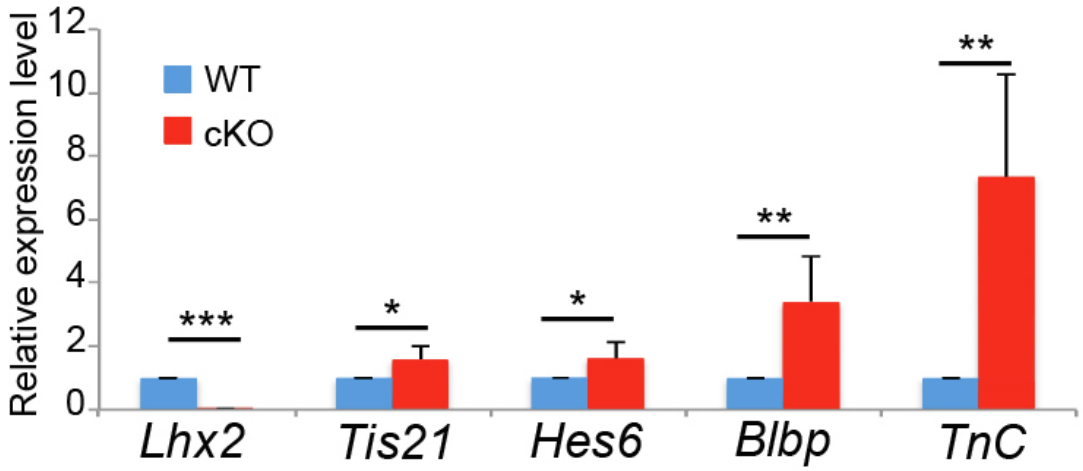

Figure S3. Lhx2 regulates the timing of neurogenesis and radial glia differentiation. (G) Quantitative RT-PCR for *Lhx2*, *Tis21*, *Hes6*, *Blbp* and *TnC* to compare the relative expression levels of these genes in E12.5 WT and cKO dorsal telencephalon. The expression of *Lhx2* is significantly down-regulated in the cKO ($p<0.001$, n=5). *Tis21* ($p<0.05$, n=4), *Hes6* ($p<0.05$, n=4), *Blbp* ($p<0.01$, n=5) and *TnC* ($p<0.01$, n=4) are significantly up-regulated in the cKO.

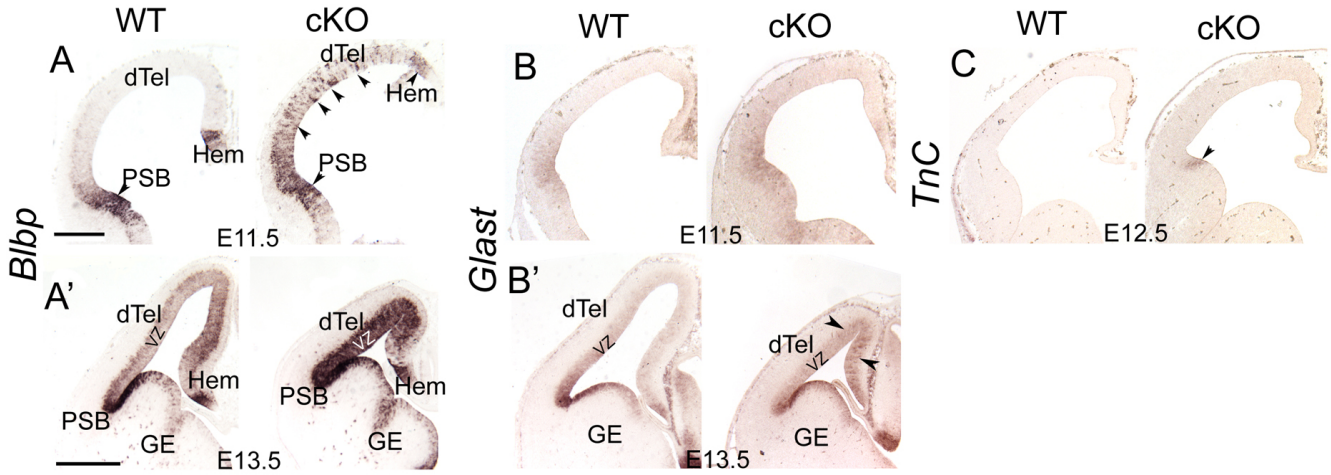

Figure S4. Expression of radial glial marker genes is up-regulated in the dorsal telencephalon of *Lhx2* cKO mice. *In situ* hybridization of *Blbp*, *Glast* and *TnC* on coronal sections from E11.5 to E13.5 WT and cKO cortices. The expression levels of *Blbp* is dramatically up-regulated (arrowheads) in the ventricular zone (vz) of dorsal telencephalon (dTel) in cKO at E11.5 (A) and E13.5 (A'). The expression level of *Glast* is similar in WT and cKO dTel at E11.5 (B), but is up-regulated (arrowheads) in cKO at E13.5 (B'). The expression of *TnC* is up-regulated in the cKO at the pallial-subpallial boundary (PSB) (arrowhead) at E12.5 (C). GE, ganglionic eminence. Scale bars, 200μm (A, B, C) and 500μm (A', B').

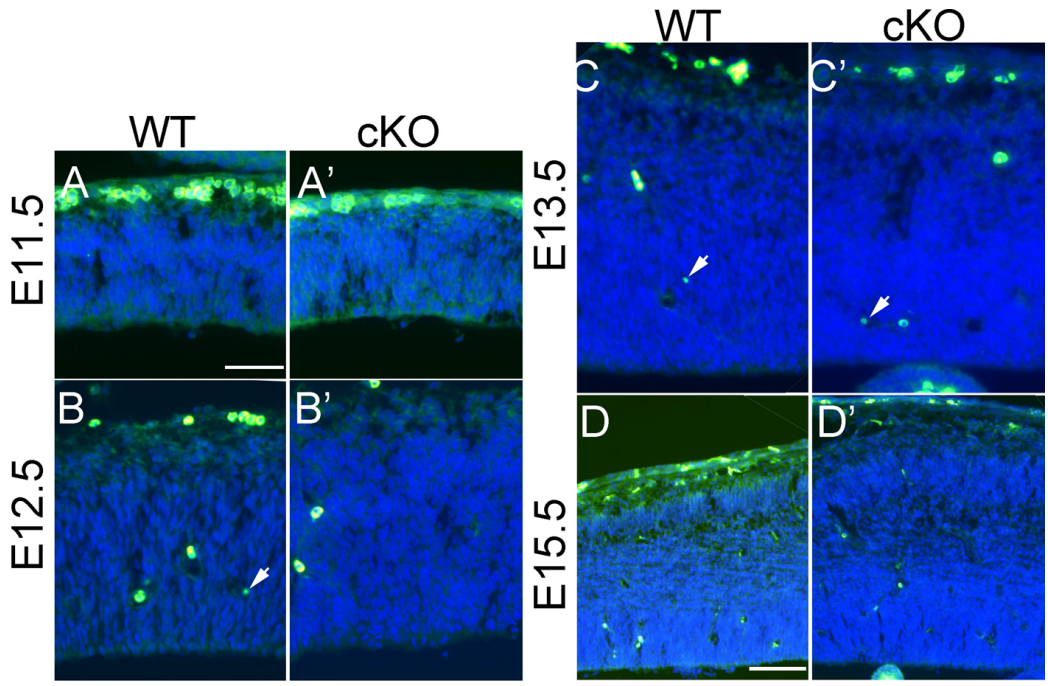

Figure S5 No detectable increase of apoptotic cells in *Lhx2* cKO dorsal telencephalon. TUNEL assays on coronal sections from E11.5 to E15.5 WT and cKO cortices. Very few apoptotic cells (arrowheads) are detected in the ventricular zone of dorsal telencephalon in WT or cKO from E11.5 to E15.5 Scale bars, 50μm (A-C') and 100μm (D, D').

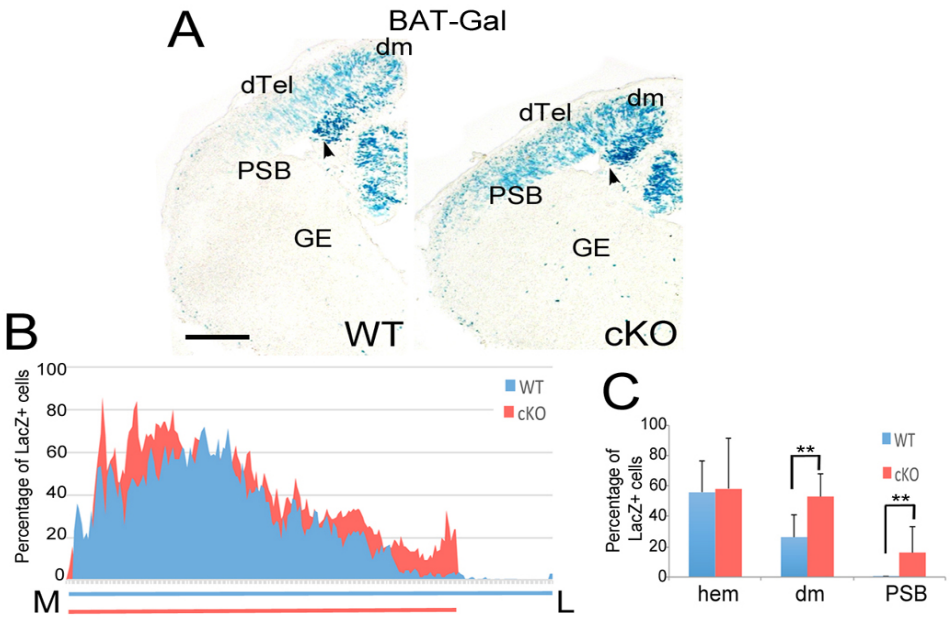

Figure S6. The β-catenin transcriptional activity is increased in *Lhx2* cKO. (A) LacZ staining of coronal sections from E13.5 WT and cKO cortex with the BAT-Gal reporter. In WT mice, β-Gal expression shows a high/medial-to-low/lateral gradient and is almost undetectable in the VZ of the most lateral dTel. In cKO mice, β-Gal expression is greatly increased, especially in the VZ of the lateral dTel. Scale bar, 250μm. Arrowheads indicate the location of cortical hem. (B) Percentage of LacZ-positive cells among total cells in 10μm wide columns from medial (M) to lateral (L) in dTel in WT (blue) and cKO (red) mice (n=3). Lines beneath the histogram represent the length of dTel from cortical hem (M) to the PSB (L) in WT (blue) and cKO (red) samples. Across the M-L axis, there was a greater number of LacZ positive cells in the cKO than in WT. (C) Comparison of relative numbers of LacZ-positive cells in WT and cKO cortex at the cortical hem or dorsal medial cortex (dm, as shown in A) or the PSB. The level of LacZ-positive cells at the hem is similar between WT and cKO samples, but a significantly larger number of LacZ-positive cells is detected in the cKO cortex at the dm and PSB relative to WT samples ($p<0.01$; n=3).

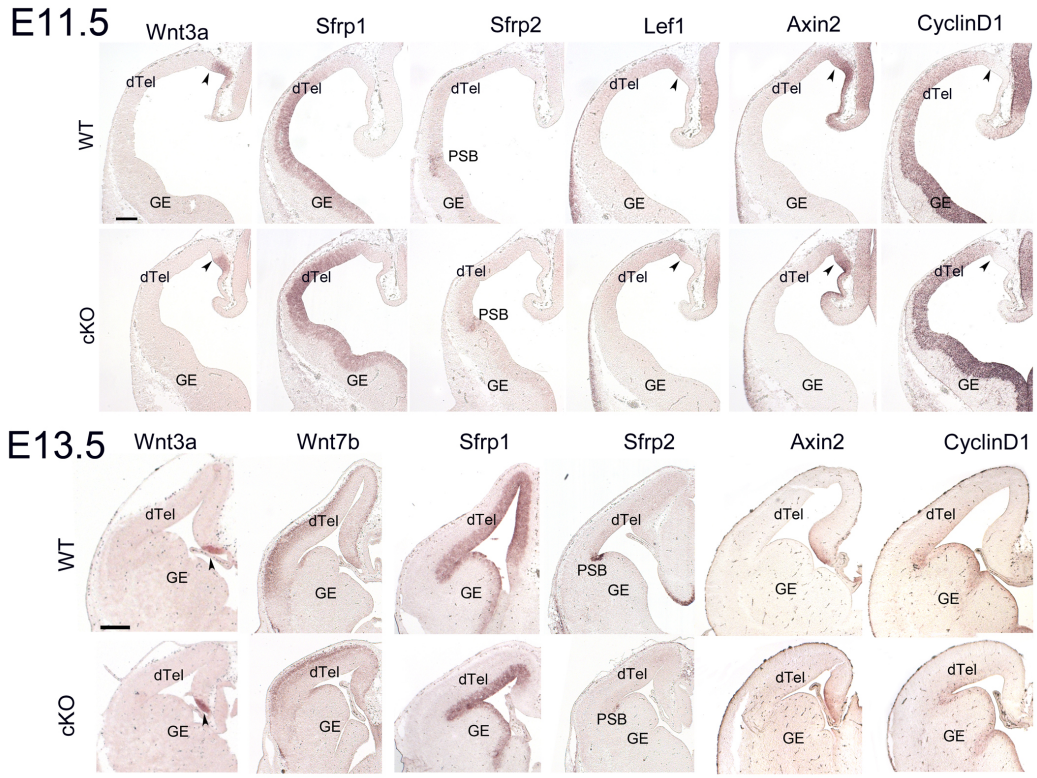

Figure S7. Expression of genes involved in Wnt signaling pathway is mostly unchanged in the dorsal telencephalon of *Lhx2* cKO mice. *In situ* hybridization of *Wnt3a*, *Wnt7b, Sfrp1, Sfrp2, Lef1 Axin2 and CyclinD1* on coronal sections from E11.5 (Top) and E13.5 (Bottom) WT and cKO cortices. The spatial expression and levels of these genes are similar in WT and cKO at both E11.5 and E13.5. The only detectable difference is that the expression of *Sfrp2* in the pallial-subpallial boundary (PSB) is decreased in the cKO at E13.5 when compared with WT. dTel, dorsal telencephalon; GE, ganglionic eminence; arrowheads: cortical hem. Scale bars, 200μm.

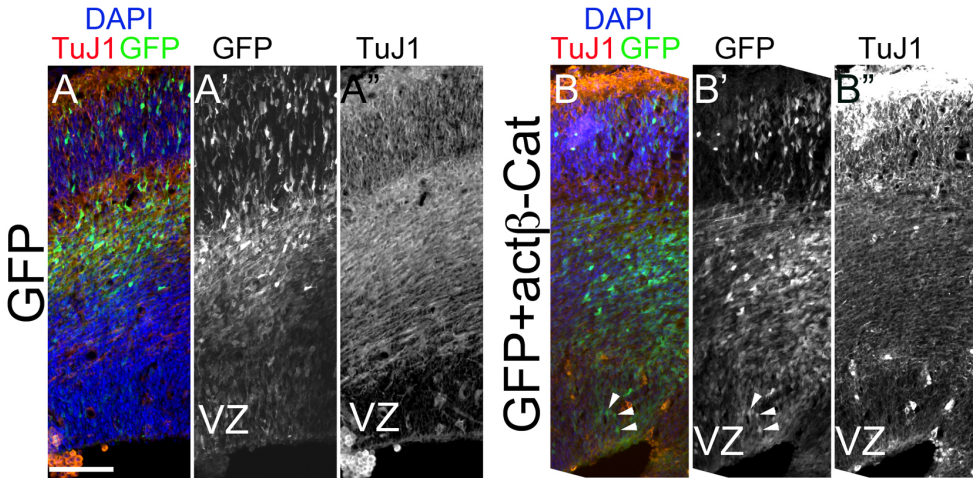

Figure S8 The expression of stabilized β-Cat maintains transfected cells in the ventricular zone in WT. Immunostaining for GFP (green) and TuJ1 (red) with DAPI staining (blue) on coronal sections of E15.5 WT and cKO dTel electroporated with GFP expression vector (A-A") or GFP expression vector

together with *nestin*-active β-Cat (B-B", as described in Figure 3). The electroporated cells are marked by GFP. The cells transfected with active β-Cat are maintained in the ventricular zone (VZ, arrowheads in B, B') and they do not express the neuronal marker, TuJ1. Scale bar, 100μm.

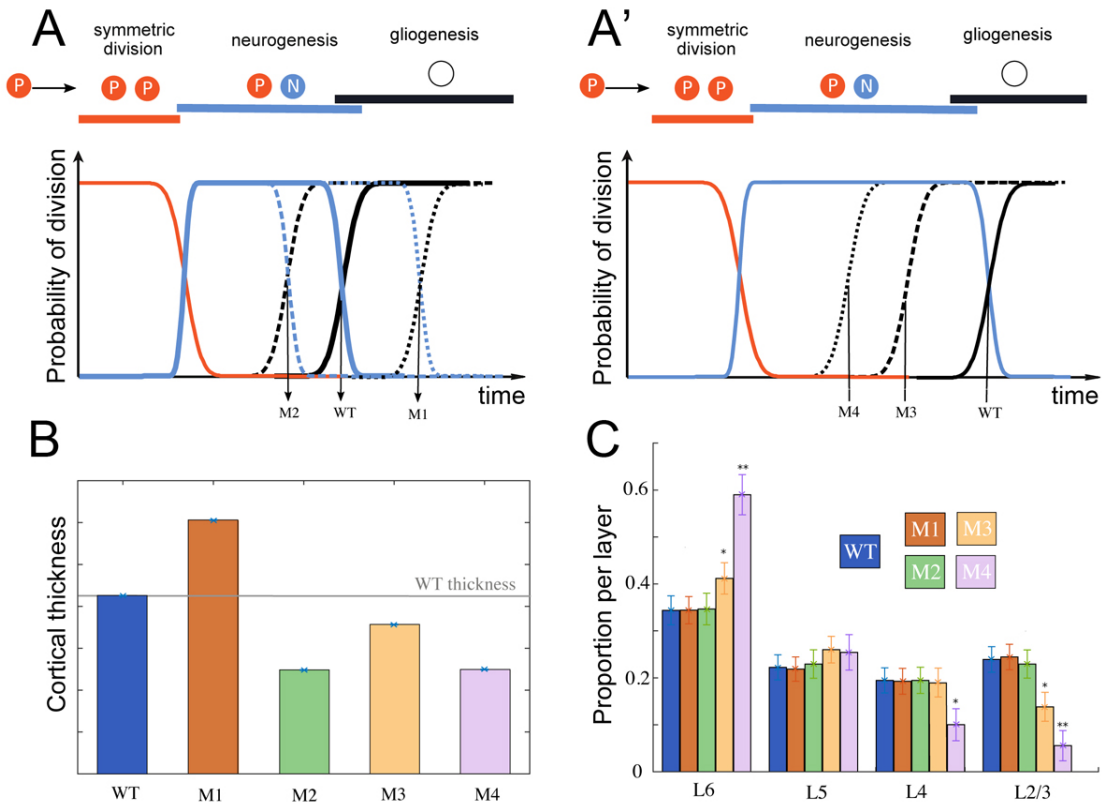

Figure S9. Role of neurogenesis timing in the thickness and layer proportions. (A) Timing of the neurogenesis in the WT model and 4 mutant models, M1 – M4. M1 and M2 differ of WT in the time progenitor switch from neurogenesis to gliogenesis, M3 and M4 have fixed neurogenesis duration but the onset of gliogenesis is advanced (see Supplementary Table 1 for parameters, the curves are illustrative here but not quantitative for legibility). (B) resulting cortical thicknesses, and (C) proportions of neurons in the different layers. Longer (resp. shorter) neurogenesis phase in the absence of precocious gliogenesis result (M1, resp. M2) in thicker (resp. thinner) cortices with no effect on the proportions of neurons in the different layers. Precocious gliogenesis reduces the cortex thickness (models M3 and M4) and imbalances the proportions of neurons in the different layers (decreased proportions in superficial layers).

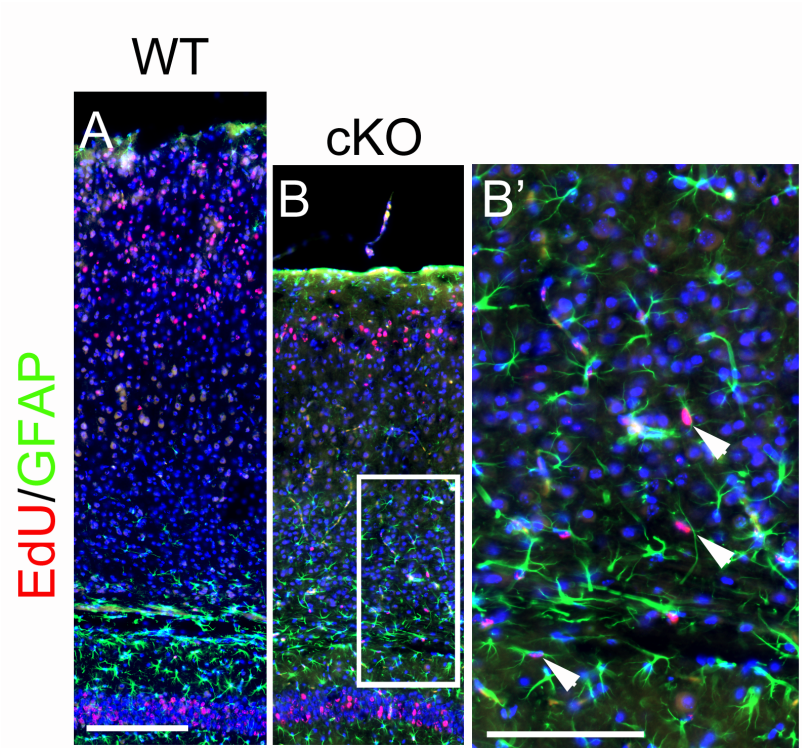

Figure S10 Precocious gliogenesis in *Lhx2* cKO cortices. Immunostaining for GFAP (green) and EdU (red) with DAPI staining (blue) on coronal sections of P15 WT and cKO cortices. EdU was injected at E17.5. (A) In WT, most of the EdU positive cells are located in the superficial layers. (B) In cKO, considerably fewer EdU positive neurons are in the superficial layers, and some EdU positive cells are found in the deep layers. (B') A higher magnification view of the inset in B. Many of the EdU positive cells in the deep layer in cKO cortices are GFAP positive glial cells. Scale bars, 100μm (A, B) and 50μm (B').